Clamping root-cutting end-effector for harvesting fresh safflower

Zhenguo Zhang[1,2*], Chao Zeng[1,2], Peng Xu[1,2], Ruimeng Shi[1,2], Yunze Wang[1,2], Zhenyu Xing[3]

(1. *College of Mechanical and Electrical Engineering, Xinjiang Agricultural University, Urumqi 830052, China*;
2. *Key Laboratory of Xinjiang Intelligent Agricultural Equipment, Xinjiang Agricultural University, Urumqi 830052, China*;
3. *College of Agriculture, Nanjing Agricultural University, Nanjing 210095, China*)

Abstract: A suitable picking method for the end-effector is the key to achieving low-damage picking. Due to the high moisture content of fresh safflower and its fragile filaments, achieving low-damage picking is a challenge for most picking robots. In this paper, a clamping and root-cutting end-effector for harvesting fresh safflower is developed. It utilizes dual rollers to pre-clamp the filaments and a blade to root-cut the safflower necking to realize the safflower harvesting operation. A mechanical model of dual rollers-blade-filaments cutting was constructed to theoretically analyze the harvesting process. The key factors affecting the performance of the end-effector were identified as blade feed speed, rotation speed, and roller clearance. Using the filament removal rate and damage rate as evaluation indices, the central composite design was carried out. The mathematical model between the test factors and evaluation indices was obtained, and the regression model was optimized with multiple objectives. Finally, the optimal combination of parameters was determined to be a blade feed speed of 40 mm/s, a rotation speed of 318 r/min, and a roller clearance of 0.60 mm. The field test was conducted under the optimal parameter combination, and the filament removal rate and damage rate were 91.25% and 5.57%, respectively. The optimized results had an error of less than 5%, indicating that the designed end-effector can harvest filaments with high removal and low damage rates. This study provides a reference for the low-damage harvesting of fresh safflower.

Keywords: harvest, end-effector, fresh safflower, clamping, root-cutting
DOI: 10.25165/j.ijabe.20251802.9461

Citation: Zhang Z G, Zeng C, Xu P, Shi R M, Wang Y Z, Xing Z Y. Clamping root-cutting end-effector for harvesting fresh safflower. Int J Agric & Biol Eng, 2025; 18(2): 146–154.

1 Introduction

Safflower (*Carthamus tinctorius L.*) is a commercial cash crop widely planted worldwide, carrying a high commercial value due to the natural pigments and active components contained within[1-3]. The mechanized harvesting of safflower filaments is a technical and seasonal work. The safflower filaments should be harvested three to five times after opening, and the harvesting period is usually only about half a month. More importantly, the flower balls must not be damaged in the process of harvesting filaments. At present, some progress has been made in the research on safflower harvesting machinery, especially in the area of end-effectors[4-6]. However, during the harvesting process of safflower, mechanical harvesting of high moisture content safflower causes a high filament damage rate and damaged fruit balls, seriously limiting the sustainable development of the safflower industry[7-9]. Therefore, ensuring the removal rate while reducing the fruit ball and filament breakage has become a technical difficulty that must be overcome in order to improve the level of mechanized safflower harvesting.

In recent years, significant progress has been made in the field of end-effector harvesting through a large number of studies by scholars[10-13], especially in the field of fruits and vegetables such as tomatoes[14,15], oranges[16,17], peppers[18], and pumpkins[19]. In research on mechanized safflower harvesting, cutting safflower necking is the most technically difficult part of the process. Safflower necking, a filament bundle formed by the growth of filaments, reflects the main biomechanical characteristics of safflower[20]. The existing harvesting methods of mechanized safflower mainly include dual rollers, comb-clamping, and cutting types. Among them, the dual rollers type has the highest removal rate of filaments but also a high damage rate. Ge et al.[21] used elastic rubber dual rollers rotating in opposite directions to draw safflower filaments. However, the filaments are easily damaged by the extrusion of the dual rollers when they pass through the clearance between the dual rollers. Zhang et al.[22] proposed a circular arc progressive method for filament harvesting. A rotary blade was used to cut the roots of the filaments, and the filaments were completely separated from the fruit bulb. Filaments were collected by negative-pressure airflow adsorption at a damage rate of 9.8%. Cao et al.[23] proposed a comb-clamping safflower filament harvesting device which used the moving teeth and fixed teeth under the action of spring preload to achieve the clamping of filaments, and completed the harvesting of filaments through spindle rotation. Although the device realizes the mechanized blind picking of filaments, the excessive impact of comb closure is likely to cause filament damage. Sun et al.[24] proposed a vertical brush-roller picking device for dry safflower harvesters. The safflower plants are gathered under the clamping action of the clamping chain and the fence frame. Under the impact and collision of the brush-roller, the fruit balls are detached from

Received date: 2024-10-26 **Accepted date:** 2025-02-19
Biographies: Chao Zeng, MS candidate, research interest: characteristic crops quality improvement and intelligent equipment, Email: chaozeng5054@163.com; **Peng Xu**, MS candidate, research interest: characteristic crops quality improvement and intelligent equipment, Email: xupeng9018@163.com; **Ruimeng Shi**, MS candidate, research interest: characteristic crops quality improvement and intelligent equipment, Email: 19199276782@163.com; **Yunze Wang**, MS candidate, research interest: characteristic crops quality improvement and intelligent equipment, Email: Wangyunze_531@163.com; **Zhenyu Xing**, MS candidate, research interest: characteristic crops quality improvement and intelligent equipment, Email: xingzhenyu151621@163.com.
***Corresponding author: Zhenguo Zhang**, Associate Professor, research interest: characteristic crops quality improvement and intelligent equipment. College of Mechanical and Electrical Engineering, Xinjiang Agricultural University, No.311, Nongda East Road, Urumqi 830052, China. Tel: +86-15099092586, Email: zhangzhenguo@xjau.edu.cn.

the filaments. Finally, the filament harvesting process is completed by negative air pressure.

According to the definition of the safflower industry, safflower with a moisture content of more than 70% is fresh[22]. However, existing harvesting devices and end-effectors predominantly utilize single-cutting or rolling methods, which are primarily designed for relatively dry safflower plants. These methods struggle to effectively harvest safflower with high moisture content. Additionally, the challenges of handling fresh, fragile safflower filaments with high moisture content further complicate the process, making low-damage picking extremely difficult for most harvesting devices. Therefore, the development of a new type of clamping and root-cutting end-effector is of great significance, as it has the potential to enhance the efficiency of fresh safflower harvesting while ensuring the quality of the crop.

In this study, a suitable picking method for harvesting fresh safflower was proposed. The clamping root-cutting end-effector has been studied and designed. The end-effector first utilizes dual rollers to pre-clamp the filaments, then a blade to root-cut the safflower necking. The quality of safflower harvesting is ensured by the smooth operation of clamping the safflower filaments and cutting the safflower necking. On this basis, the mechanical models of the dual rollers-filaments and blade-filaments were constructed. A theoretical analysis of the clamping and cutting process was carried out to determine the critical factors affecting the performance of the end-effector. With the filament removal rate and filament damage rate as evaluation indices, the optimal parameter combination of the end-effector was obtained by carrying out the central composite design and field tests. The results provide a reference for harvesting safflower with high moisture content and low-damage picking, and also contribute to the mechanized harvesting of other similar crops.

2 Materials and methods

2.1 Material features of safflower

The physical properties of safflower serve as a basis for the design of safflower harvesting devices. Yunhong No. 6, a safflower widely grown in China, was used as the test material. The samples were obtained from the Yunguang Safflower Cultivation Agricultural Cooperative in Ili Kazakh Autonomous Prefecture, China. The structure of safflower consists mainly of filament, necking, and fruit ball[25], in which necking is defined as the position of interaction with the shear mechanism, as shown in Figure 1a.

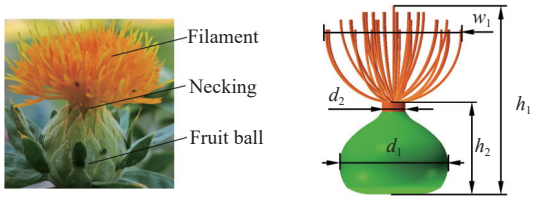

a. Composition of the safflower b. Safflowergeometric parameters

Figure 1 Composition of safflower and its key geometric parameters

The key geometric parameters of the safflower, including filament width w_1, safflower height h_1, fruit ball height h_2, fruit ball diameter d_1, and necking diameter d_2, are shown in Figure 1b.The three-dimensional parameters of safflower were measured using the Vernier scale (DL92150P, range 0-150 mm, accuracy 0.01 mm, developed by Deli Group Co., Ltd.). The average density of safflower (wet basis) was 400 kg/m^3 as measured by a measuring cylinder (range 0-500 mL, accuracy 5 mL, developed by Fuzhou North Glass Experimental Instrument Co., Ltd.) and an electronic scale (I-2000, range 0-500 g, accuracy 0.01 g, developed by Deqing Bayjie Electric Appliance Co., Ltd.). The measurement results are listed in Table 1.

Table 1 Main material feature parameters of safflower

Parameters	Range/mm	Mean/mm
w_1	31.15-45.99	39.25±4.17
h_1	35.89-46.52	41.73±3.07
h_2	18.64-25.34	22.79±1.61
d_1	22.40-29.55	25.46±1.85
d_2	3.17-5.79	4.52±0.71
ρ	385.45-432.77	400±11.07

2.2 Structure and working principle of the safflower harvesting robot

As shown in Figure 2, the structure of the safflower harvesting robot includes a moving system, a filament collection system, a clamping root-cutting end-effector, a spatial positioning system, a central control system, a power system, etc. The working principle is as follows: The clamping and root-cutting end-effector is fixedly connected to the spatial positioning system. The central control system adjusts the position of the whole machine and the end-effector after obtaining information about the spatial position of the safflower plant. The spatial positioning system aligns the end-effector with the safflower fruit ball. The end-effector utilizes dual rollers to pre-clamp the filaments and the blades to root-cut the safflower necking. Finally, the cut filaments are collected under the negative pressure airflow of the filament collection system.

As shown in Figure 3, the end-effector consists of a clamping mechanism, a root-cutting mechanism, a slide mechanism, a machine casing, a rack mechanism, a stepping motor, etc. According to the filament movement state, the safflower harvesting process is divided into four working stages. In the first stage, the central control system adjusts the position of the end-effector. The spatial positioning system moves the end-effector to the top of the safflower fruit ball, as shown in Figure 2a. In the second stage, the spatial positioning system continues to move downward. The filaments are rolled and kept in a vertical state by the action of negative pressure airflow. At the same time, the filament spreading decreases significantly. The filaments are rolled into the clamping mechanism, and the root-cutting mechanism is in the open state, as shown in Figure 2b. In the third stage, the central control system activates the stepping motor of the root-cutting mechanism. The root-cutting mechanism cuts the safflower necking, and the filaments are separated from the fruit bulb, as shown in Figure 2c. In the final stage, the filaments are entirely rolled into the clamping mechanism. Finally, the filaments enter the filament collection box under the influence of the negative airflow, as shown in Figure 2d.

2.3 Design of key components

2.3.1 Method of picking safflower

Selecting the proper picking method is one of the critical factors in improving operational efficiency and harvest success. The picking method for safflower is the basis and prerequisite for designing the end-effector[26,27]. The picking method is determined according to the morphological characteristics of safflower, and the mechanical structure design of the end-effector is provided for reference [28].

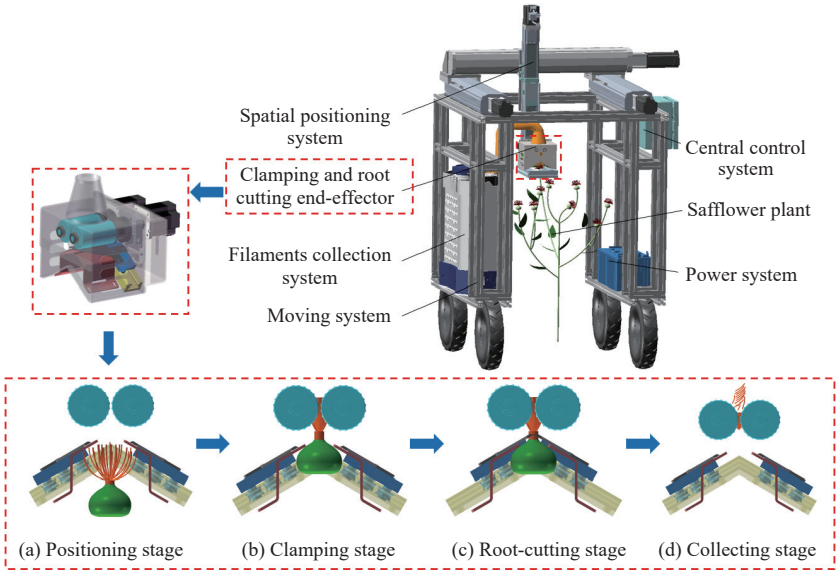

Figure 2 Structure of the safflower harvesting robot

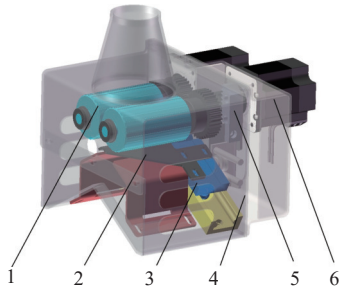

1. Clamping mechanism 2. Root-cutting mechanism 3. Slide mechanism 4. Machine casing 5. Rack mechanism 6. Stepping motor

Figure 3 Structure of the clamping root-cutting end-effector

The clamping mechanism and root-cutting mechanism are the core components of the end-effector. The key components that determine the effect of filament clamping and root-cutting are shown in the structure of Figure 4. It mainly consists of dual rollers, a root-cutting blade, a blade holder, a blade slide, and a support plate. During the harvesting operation, the clamping mechanism realizes safflower pre-clamping. Subsequently, the root-cutting blade of the root-cutting mechanism moves along the blade slide to realize the safflower filament cutting. Finally, the filament collection system collects the safflower filaments through a negative-pressure airflow.

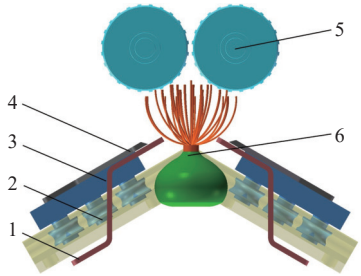

1. Dual rollers 2. Blade 3. Blade holder 4. Holder slide 5. Support plate 6. Safflower

Figure 4 Structure of the clamping and root-cutting mechanism

2.3.2 Design of clamping components

The clamping mechanism is the key working component to realize safflower clamping, which determines the clamping effect of the end-effector and the damage to the safflower filaments. The clamping mechanism mainly consists of a pair of rubber rollers, and each of them rotates in the opposite direction at the same speed. As the end-effector moves over the safflower plant, the blooming filaments are rolled into the clamping mechanism and constrained together to form a filament bundle. The filament bundle is assumed as an ellipsoidal rigid body with uniform mass. During the movement of the filament bundle, it is not interfered with by outside factors, and the external forces are all acting on the center of mass[29,30]. With the center of mass of the filament bundle as the origin, a plane right-angle coordinate system is established. In this case, the horizontal direction to the right is the positive direction of the x-axis, and the vertical direction up is the positive direction of the y-axis.

The mechanical analysis of the dual rollers-filament bundle is shown in Figure 5. Combining kinematics and dynamics theories, a mechanical model of the dual rollers-filament bundle interaction is established. The filament bundle motion is taken as a fixed-axis movement, ignoring the centrifugal and Cole forces generated by the rotating pair of dual rollers. According to D'Alembert's principle, the following equations are established by mechanical analyses:

$$\begin{cases} \sum F_x = F_2\sin\alpha + N_2\cos\alpha - N_1\cos\beta - F_1\sin\beta = 0 \\ \sum F_y = F_1\cos\beta + F_2\cos\alpha - N_1\sin\beta - N_2\sin\alpha - G = 0 \\ G = mg \\ F_1 = N_1 f \\ F_2 = N_2 f \end{cases} \tag{1}$$

When the filament bundle is rolled between dual rollers for self-rotation, the filament bundle is not moved along the x-axis in the positive and negative directions. The following equations are established:

$$\begin{cases} \sum M_A \geq 0 \\ \sum M_B \leq 0 \end{cases} \tag{2}$$

$$\begin{cases} \sum M_A = F_1 a\sin\left[90^\circ - (\alpha+\beta)\right] - N_1 a\cos\left[90^\circ - (\alpha+\beta)\right] - \\ \qquad Ga\cos\alpha \geq 0 \\ \sum M_B = F_2 b\sin\left[90^\circ - (\alpha+\beta)\right] - N_2 b\cos\left[90^\circ - \alpha + \beta\right] - \\ \qquad Gb\cos\beta \leq 0 \end{cases} \tag{3}$$

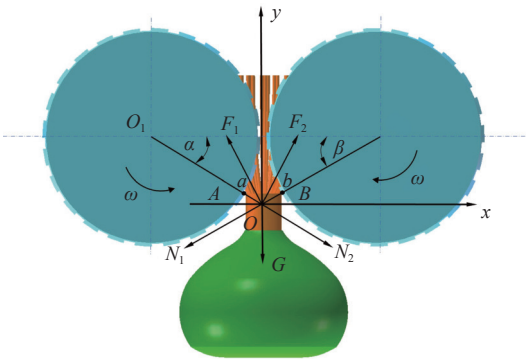

Note: ω is the dual rollers speed, r/min; O is the center of mass of the filament bundle; O_1 and O_2 are the center points of the left and right rollers, respectively; F_1 and F_2 are the left and right friction forces between the filament bundle and the dual rollers, respectively, N; N_1 and N_2 are the left and right normal forces of the filament acting on the dual rollers, respectively, N; G is filament bundle gravity, N; α is the angle between line O_1O_2 and line OO_1, (°); β is the angle between line O_1O_2 and line OO_2, (°); A and B are the left and right contact points of the filament bundle on the dual rollers, respectively; a is the distance between point A and point O, mm; b is the distance between point B and point O, mm.

Figure 5 Mechanical analysis of the dual rollers-filament bundle

Simplifying Equation (3) establishes Equation (4):

$$\begin{cases} N_1 \le \dfrac{G\cos\alpha}{\sin(\alpha+\beta)-f\cos(\alpha+\beta)} \\ N_2 \ge \dfrac{G\cos\beta}{\sin(\alpha+\beta)-f\cos(\alpha+\beta)} \end{cases} \tag{4}$$

In summary, the mechanical analyses show that the normal force of the filament bundle is related to the shape, gravity, roller clearance, and coefficient of friction between the safflower and the material. Of the above factors, the roller clearance can be adjusted independently. Therefore, the roller clearance is selected as the key influencing factor.

2.3.3 Design of root-cutting components

The safflower-cutting operation directly affects the removal rate and damage rate of filaments. The safflower necking denotes the formation of an overflow of filament bundle, which reflects the main mechanical characteristics of safflower. Through the mechanical analysis of the root-cutting blade-safflower necking interaction, the mechanical model of the safflower-cutting process is established to provide theoretical support for the design of the root-cutting mechanism.

During the movement of the filament bundle, it is assumed that it is not disturbed by external factors, and the external forces are acting on the center of mass of the safflower necking. The safflower necking acquires the velocity imparted by the root-cutting blade, generating acceleration and inertial forces in opposite directions. Considering the different accelerations and inertial forces at each point on the safflower necking, the combined force of all inertial forces can be regarded as concentrated at the center of mass. According to the blade cutting theory, the cutting process of safflower necking is shown in Figure 6. The following equations are established.

$$\begin{cases} F_T = \sum F_g + F_w + F_N \\ F_q = F_T\cos\varphi \end{cases} \tag{5}$$

$$F_q = \left(\sum F_g + F_w + F_N\right)\cos\varphi \tag{6}$$

where, F_T is the cutting force on the safflower necking, N; $\sum F_g$ is the resultant force of the inertial forces of the safflower filaments, N; F_w is the bending reaction force of safflower necking, N; F_N is the friction force between the safflower necking and the blade, N; F_q is the cutting force that cuts off the necking, N; φ is the angle between the cutting direction and the horizontal direction, (°).

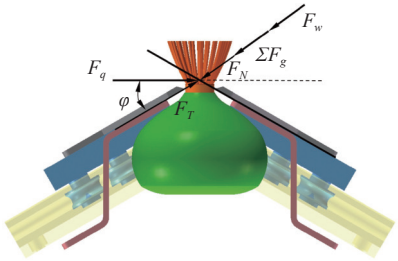

Figure 6 Cutting process of safflower necking

According to Equations (5) and (6), the safflower filament is cut off as the product of the cutting force, and the cosine value φ is greater than the cutting force on the necking ($F_T\cdot\cos\varphi \ge F_q$). To deeply analyze the cutting process of the blade, assume the cross-section of the cutting of safflower necking is either a square circle or an ellipse. In the process of cutting the safflower necking with a root-cutting blade, the safflower necking is parallel to the plane of the blade, and the cutting cross-section is a square circle. The safflower necking is at an angle to the plane of the blade, and the cutting cross-section is elliptical. During the operation of the root-cutting mechanism, the filaments are rolled into the dual rollers. With the root-cutting mechanism driven, the root-cutting blade moves along the blade slide, colliding with the safflower necking and cutting it off. According to the momentum theorem, the safflower necking is impacted by the root-cutting blade. The following Equation (7) is established:

$$F_T t = mv \tag{7}$$

where, t is cutting time, s; m is the mass of filament bundle, kg; v is the blade feed speed, mm/s.

Since both safflower filaments and fruit balls are elastic materials, the safflower necking will be elastically deformed when subjected to the impact force. The contact area between the root-cutting blade and the safflower necking increases after local deformation. Using the right root-cutting blade as an example, the contact point of the root-cutting blade with the safflower necking is set to point Q. With the contact point Q as the origin, a plane right-angle coordinate system is established. The horizontal direction to the left is the positive direction of the x-axis, and the vertical direction up is the positive direction of the y-axis, as shown in Figure 7. The blade feed speed is kept constant during the cutting process. The following Equation (8) is established:

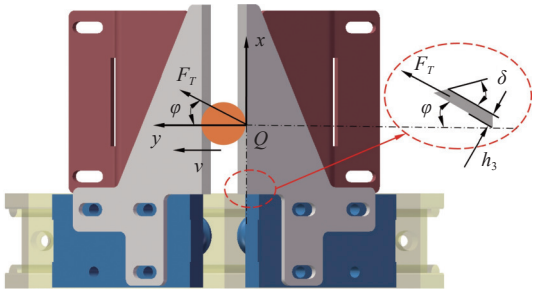

Note: δ is inclination angle of the blade, (°); h_3 is thickness of the blade, mm.

Figure 7 Mechanical analysis of root-cutting blade-safflower necking interaction

$$L = vt \tag{8}$$

where, L is the depth of the blade feed, mm.

Assuming that the root-cutting blade impact load is acting entirely on the safflower necking, the critical conditions for safflower filament cutting separation can be given by Equation (9):

$$F_T \geq \sigma_s A_1 \tag{9}$$

where, σ_s is the maximum stress of safflower necking separation, Pa; A_1 is the area of blade cutting necking, mm^2.

Ignoring the curvature of the contact surface between the root-cutting blade and the safflower necking, the action area of the safflower filament is given by Equation (10):

$$A_1 = 2h_3 L \frac{\tan\frac{\delta}{2}}{\cos\varphi} \tag{10}$$

The separation critical Equation (11) for safflower necking was obtained by combining Equations (8), (9), and (10):

$$\frac{F}{A_1} = \frac{mv^2\cos\varphi}{2h_3L^2\tan\frac{\delta}{2}} \geq \sigma_s \tag{11}$$

From Equation (11), it can be seen that the separation condition of safflower necking is related to the blade feed speed. To achieve safflower necking separation and reduce the filament damage rate, it is essential to choose the right blade feed speed. The approximate calculation of the ultimate stress leads to Equation (12):

$$\sigma_s = \frac{F_{Tm}}{A_s} \tag{12}$$

where, F_{Tm} is the maximum cutting force of blade to cut necking, N; A_s is the maximum area of blade cutting necking, mm^2.

According to Equations (11) and (12), the blade feed speed should satisfy Equation (13) to cut off the safflower necking:

$$v \geq \sqrt{\frac{2h_3L^2F_{Tm}\tan\frac{\delta}{2}}{A_s m\cos\varphi}} \tag{13}$$

In summary, the blade feed speed directly affects the operating effect on safflower filaments and necking. With the increase of the blade feed speed, the cutting force required for safflower necking cutting decreases. However, increasing the blade feed speed also led to an increased impact on the safflower necking, resulting in a higher rate of filament damage. In addition, the determination of the blade feed speed is also related to the cutting edge, blade thickness, and other factors. Therefore, when designing the root-cutting mechanism, the relationship between the blade feed speed and structural parameters should be considered comprehensively.

2.4 Test methods

2.4.1 Pre-tests indoors

Before the field trials, pre-tests of key components and related parameters were conducted indoors. The test equipment was a safflower harvesting robot (made by the team), which mainly included a moving system, a filament collection system, a clamping root-cutting end-effector, a spatial positioning system, a central control system, a power system, etc., as shown in Figure 8. The test instruments mainly included LA114 electronic analytical balance (Shanghai Zanwei Weighing Instrument Co., Ltd., range 0-110 g, accuracy 0.1 mg), Vernier calipers (Wenzhou Maikelen Electric Co., Ltd., range 0-150 mm, accuracy 0.02 mm), TMS-TM, and DLY-2301 tachometer (Dexerial Group Co., Ltd., range 2.5-99 999 rpm, accuracy 0.1 r/min), and so on.

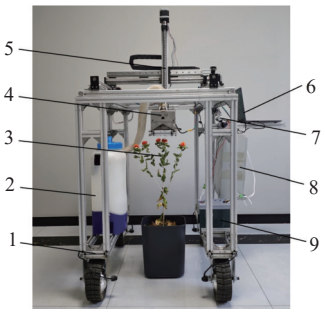

1. Moving system 2. Filament collection system 3. Safflower plant 4. Clamping and root-cutting end-effector 5. Spatial positioning system 6. Computer 7. Vision camera 8. Central control system 9. Power system

Figure 8 Fresh safflower harvesting robot

2.4.2 Test factors

(1) Rotation speed X_1

When the dual rollers rotate at high speed, the air is moving at a higher speed and the pressure is smaller. Therefore, a negative pressure airflow field is formed, which produces an adsorption effect on the safflower. The higher the speed of the dual rollers, the stronger the adsorption capacity of safflower. Through the pre-test, the safflower can be picked when the speed of the dual rollers is greater than or equal to 250 r/min. Considering the stability and reliability of mechanical work, the speed of the dual rollers was selected as 250-400 r/min.

(2) Roller clearance X_2

The roller clearance directly affects the feeding speed and the separation effect of safflower and fruit balls. The larger the roller clearance, the more the safflower effective feeding speed increases. However, the positive pressure and friction of the rollers on the safflower are reduced accordingly. A roller clearance that is too large causes the safflower to fail to separate from the fruit ball. The smaller the clearance between the rollers, the more the safflower is subjected to the squeezing force and friction of the dual rollers. According to the measurements of the safflower necking in Table 1, the roller clearance was selected as 0.4-0.8 mm.

(3) Blade feed speed X_3

The blade feed speed is the key factor affecting the damage rate of safflower filament. The faster the blade feed speed, the higher the filament damage rate. Through the pre-tests, the cutting speed v was at 20-40 mm/s, which has a better harvesting effect. In this test device, considering the stability and reliability of mechanical work, the blade feed speed was selected as 20 mm/s and 40 mm/s.

2.4.3 Response index

(1) Filament removal rate y_1

For a random group of 10 safflowers, the percentage of the mass of filaments picked to the total mass of filaments was defined as the filament removal rate. The Equation (14) is as follows:

$$y_1 = \frac{m_1}{m_1 + m_2} \times 100\% \tag{14}$$

where, m_1 is the mass of filaments picked from a single group of fruit balls, g; m_2 is the mass of filaments not picked on a single group of fruit balls, g.

(2) Filament damage rate y_2

For a random group of 10 safflowers, the percentage of the mass of filaments picked and broken to the total mass of filaments was defined as the filament damage rate. The Equation (15) is as follows:

$$y_2 = \frac{m_3}{m_1} \times 100\% \tag{15}$$

where, m_3 is the mass of broken filaments in a single group of harvested filaments, g.

2.4.4 The central composite design

To reduce experimental errors and clarify the interrelationships among factors, the central composite design was adopted. The test parameter codes are shown in Table 2. Each numeric factor was set to five levels, plus and minus alpha (axial points), plus and minus 1 (factorial points), the center points, and the bonding parameter code.

Table 2 Parameter codes of the test design

Code	Parameter		
	Rotation speed X_1/(r·min^{-1})	Roller clearance X_2/(mm)	Blade feed speed X_3/(mm·s^{-1})
−1.682	198.87	0.26	13.18
−1	250.00	0.40	20.00
0	325.00	0.60	30.00
1	400.00	0.80	40.00
1.682	451.13	0.94	46.82

3 Results and discussion

3.1 Results of the central composite design

The test program and results are shown in Table 3, with a total of 21 groups of tests. These included 14 analytical factors and 7 null estimation errors, with groups 1 to 14 being analytic factor design tests and groups 15-21 being central design tests[31].

The results of variance analysis are shown in Table 4. Analyzing the variance by Design-Expert, the regression models of filament removal rate y_1 and filament damage rate y_2 on the rotation speed X_1, the roller clearance X_2, and the blade feed speed X_3 were established. The p-values of the regression models for the filament removal rate and filament damage rate were less than 0.01, indicating that the relationship between the regression equations and the response indices was highly significant. The p-values of the lack of fit terms for the filament removal rate and filament damage rate were 0.67 and 0.43, respectively. These values are both greater than 0.05, indicating that the lack of fit terms were not significant and the regression equations were not fitted.

Table 3 Results of the central composite design

No.	Test parameters and levels			Response indices	
	Rotation speed X_1/r·min^{-1}	Roller clearance X_2/mm	Blade feed speed X_3/mm·s^{-1}	Removal rate y_1/%	Damage rate y_2/%
1	250	0.4	20	88.76	5.36
2	400	0.4	20	91.29	7.01
3	250	0.8	20	86.87	4.81
4	400	0.8	20	90.09	5.67
5	250	0.4	40	90.75	5.74
6	400	0.4	40	92.75	7.42
7	250	0.8	40	87.54	4.85
8	400	0.8	40	90.77	6.02
9	218.93	0.6	30	87.56	4.75
10	431.06	0.6	30	91.18	6.77
11	325	0.263 641	30	91.54	6.88
12	325	0.936 359	30	87.81	4.9
13	325	0.6	13.1821	89.55	4.91
14	325	0.6	46.8179	91.44	5.4
15	325	0.6	30	91.15	5.02
16	325	0.6	30	90.31	5.05
17	325	0.6	30	90.68	5.16
18	325	0.6	30	90.26	5.36
19	325	0.6	30	90.39	5.25
20	325	0.6	30	90.89	5.51
21	325	0.6	30	90.72	4.99

Table 4 Variance analysis of experimental results

Source of variation	Degree of freedom	Removal rate y_1				Damage rate y_2			
		Quadratic sum	Mean square	F-value	p-value	Quadratic sum	Mean square	F-value	p-value
Model	9	46.72	5.19	56.83	< 0.01**	12.41	1.38	34.57	< 0.01**
X_1	1	21.33	21.33	233.53	< 0.01**	5.62	5.62	140.81	< 0.01**
X_2	1	15.51	15.51	169.78	< 0.01**	4.13	4.13	103.55	< 0.01**
X_3	1	4.66	4.66	51.03	< 0.01**	0.2941	0.2941	7.37	0.0201*
X_1X_2	1	0.4608	0.4608	5.04	0.0462*	0.2113	0.2113	5.30	0.0419*
X_1X_3	1	0.0338	0.0338	0.3700	0.5553	0.0144	0.0144	0.3623	0.5594
X_2X_3	1	0.5513	0.5513	6.03	0.0319*	0.0200	0.0200	0.5015	0.4936
X_1^2	1	2.82	2.82	30.92	0.0002**	0.9375	0.9375	23.51	0.0005**
X_2^2	1	1.59	1.59	17.46	0.0015**	1.31	1.31	32.95	0.0001**
X_3^2	1	0.0195	0.0195	0.2138	0.6528	0.0195	0.0195	0.4882	0.4992
Residual	11	1.00	0.0913			0.4387	0.0399		
Lack of fit	5	0.3593	0.0719	0.6680	0.6627	0.2144	0.0429	1.15	0.4286
Pure error	6	0.6455	0.1076			0.2243	0.0374		
Total	20	47.73				12.85			

Note: highly significant ($p < 0.01$), significant ($0.01 \le p < 0.05$).

The analysis of variance for the filament removal rate y_1 showed that the effects of factors X_1, X_2, X_3, X_1^2, and X_2^2 were highly significant (p<0.01). The effects of factors X_1X_2 and X_2X_3 were significant ($0.01 \le p < 0.05$), and the rest of the factors were not significant. The analysis of variance for the filament damage rate y_2 showed that the effects of factors X_1, X_2, X_1^2, and X_2^2 were highly significant (p<0.01). The effects of factors X_3 and X_1X_2 were significant ($0.01 \le p < 0.05$), and the rest of the factors were non-significant. To ensure the accuracy of the response surface, the significant factors were retained. The regression equations for the filament removal rate y_1 and filament damage rate y_2 are shown in Equations (16) and (17), respectively:

$$y_1 = 75.16 + 0.06X_1 + 3.12X_2 + 0.19X_3 + 0.02X_1X_2 - 0.13X_2X_3 - 8.15X_2^2 \quad (16)$$

$$y_2 = 9.29 - 0.02X_1 - 7.36X_2 - 0.01X_3 - 0.01X_1X_2 - 0.03X_2X_3 + 7.4X_2^2 \quad (17)$$

3.2 Discussion of the central composite design

According to the regression Equations (16) and (17), the response surfaces of the test factors on the filament removal rate y_1 and filament damage rate y_2 were established. The steepness of the response surface reflects the influence degree of interaction terms on the response values. The steeper the response surface, the greater the influence of the interaction term on the response value[32] .

The response surface of significant factor interactions on the filament removal rate was established. As shown in Figure 9a, the filament removal rate increases with the increase of the rotation speed. However, the roller clearance is opposite to the rotation speed. The increasing trend of rotation speed is steeper than roller clearance. This indicates that increasing the rotation speed and decreasing the roller clearance increased the removal rate. The significance of rotation speed is significantly greater than roller clearance.

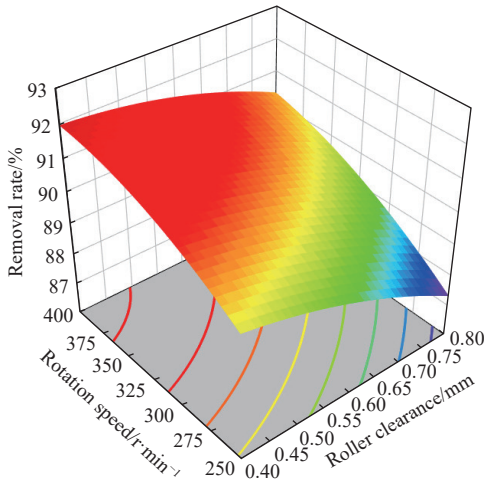

a. Effects of X_1 and X_2

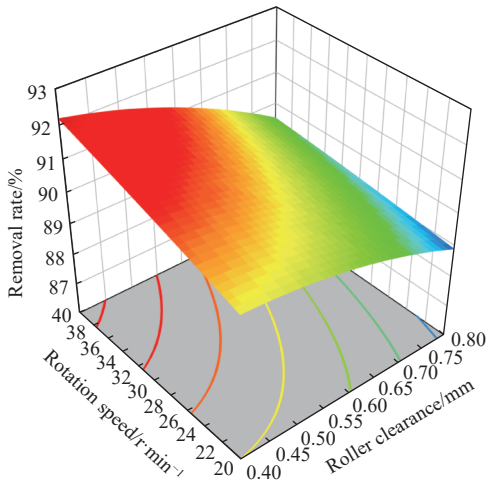

b. Effects of X_2 and X_3

Figure 9 Interaction effects of significant factors on filament removal rate

As shown in Figure 9b, the filament removal rate increases as the blade feed speed increases. The increasing trend of roller clearance is steeper than the blade feed speed. This indicates that increasing blade feed speed also increased the removal rate. The significance of roller clearance was significantly greater than blade feed speed. Considering the three parameters together, the sequence of influence for the removal rate, from greatest to least, is rotation speed, roller clearance, and blade feed speed. To satisfy the requirement of a filament removal rate over 91%, the blade feed speed is more than 25 mm/s, the rotation speed is more than 300 r/min, and the roller clearance is less than 0.7 mm.

The response surface of significant factor interactions on the filament damage rate was established, as shown in Figure 10. The faster the blade feed speed, the higher the filament damage rate. However, the roller clearance is opposite to the rotation speed. The increasing trend of rotation speed is steeper than roller clearance. The observed trend was similar to Figure 9a, but the response surface of Figure 10 was higher in steepness. This indicates that both decreasing the rotation speed and increasing the roller clearance decreased the filament removal rate. The significance of the rotation speed was also greater than the roller clearance for the filament damage rate. To satisfy the requirement of a filament damage rate under 6%, the rotation speed is less than 325 r/min and the roller clearance is more than 0.5 mm.

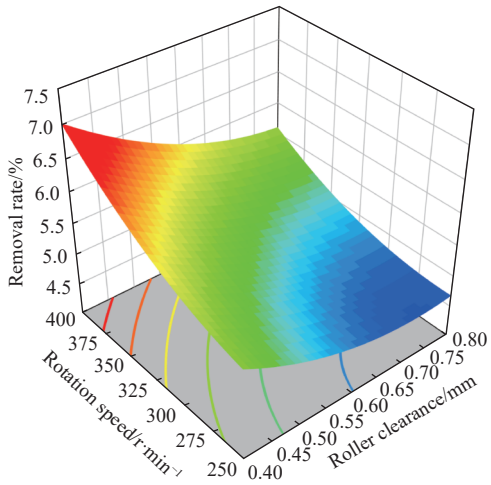

Figure 10 Interaction effect of X_1 and X_2 on filament damage rate

3.3 Parameter optimization and test validation

3.3.1 Parameter optimization

According to the response analysis, the factors had different effects on the filament removal rate and filament damage rate. Therefore, the optimal combination of parameters required for filament harvesting performance was obtained by a multi-objective optimization approach. The requirements of the highest filament removal rate and the lowest filament damage rate were taken as the optimization objectives. The objective function and constraints for planning are shown in Equation (18):

$$\begin{cases} \max y_1(X_1, X_2, X_3) \\ \min y_2(X_1, X_2, X_3) \\ \text{s.t.} \begin{cases} 300 \text{ r/min} \le X_1 \le 325 \text{ r/min} \\ 0.5 \le X_2 \le 0.7 \\ 25 \text{ mm/s} \le X_3 \le 40 \text{ mm/s} \end{cases} \end{cases} \tag{18}$$

Using Design-Expert software to solve Equation (18), the best parameter combination of the influencing factors was obtained as follows: a rotation speed of 318 r/min, a roller clearance of 0.6 mm, and a blade feed speed of 40 mm/s. In this case, the optimized parameters of the filament removal rate and filament damage rate were obtained as 91.06% and 5.31%, respectively.

3.3.2 Test validation

The field verification test was conducted from July 26 to July 30, 2024, at the Yunguang Safflower Cultivation Agricultural Cooperative in Xinjiang, China, as shown in Figure 11. The test

operating conditions and methods are the same as the above tests. The test was conducted with a rotation speed of 318 r/min, a roller clearance of 0.6 mm, and a blade feed speed of 40 mm/s. To eliminate random errors, the test was repeated five times for each parameter combination. The end-effector and harvesting effects are shown in Figs. 11a and 11b, respectively. The average values of the five groups of tests were taken as the test results, which were a filament removal rate of 91.25% and a filament damage rate of 5.57%. The relative errors with the predicted values were not more than 5%, and the theoretical values were similar to the actual values. The accuracy of the model was verified, and the optimal parameter combination could meet the practical application requirements.

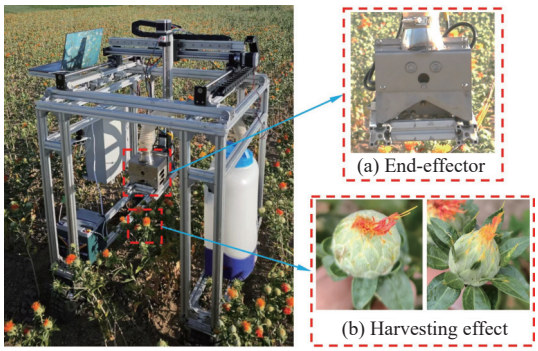

Figure 11 Field verification test

4 Conclusions

To solve the problems of the harvesting of fresh safflower with high moisture content, a new type of clamping root-cutting end-effector for fresh safflower filament harvesting was studied and designed. Through theoretical analyses and calculations, a mechanical model of roller-blade-filament cutting was constructed. The end-effector utilizes the dual rollers to pre-clamp the filaments, then the blade to root-cut the safflower necking. The quality of safflower harvesting is ensured by the smooth operation of clamping the safflower filaments and cutting the safflower necking. Accordingly, the following conclusions are drawn:

(1) Based on the design of dual rollers for clamping and a blade for root-cutting, a clamping and root-cutting end-effector for harvesting fresh safflower was developed. It utilizes the dual rollers to pre-clamp the filaments, then the blade to root-cut the safflower necking. Through theoretical analysis of the clamping and cutting process, a mechanical model of roller-tool-filament cutting was constructed. The results of the analysis can be used as a reference for improving the end-effector structure and optimizing the operating parameters.

(2) The central composite design was performed on a self-constructed safflower harvesting robot. Using Design-Expert software to establish the response surface, the effects of rotation speed, roller clearance, and blade feed speed on the filament removal rate and filament damage rate, respectively, were analyzed. The optimized parameters of the filament removal rate and filament damage rate were 91.06% and 5.31%, respectively. In this case, the rotation speed is 318 r/min, the roller clearance is 0.6 mm, and the blade feed speed is 40 mm/s.

(3) Under the optimal parameter combination, the field verification test was carried out. The results showed that the filament removal rate and filament damage rate were 91.25% and 5.57%, respectively. The relative errors with the predicted values were not more than 5%. The measured and predicted values of each index were relatively consistent, indicating that the results of parameter optimization were reliable.

This study provides a reference for harvesting safflower with high moisture content and low-damage picking. It is also helpful for the mechanized harvesting of other similar crops. In the field harvesting process, the optimization parameters were adjusted and optimized based on actual application scenarios. Further studies are needed to address the disturbing factors affecting safflower plants, such as different filament morphologies and the growth attitudes of safflower plants.

Acknowledgements

This work was supported by the National Natural Science Foundation of China (Grants No. 32460449, 52265041, and 31901417). The authors also acknowledge the Central Guidance for Local Science and Technology Development Funding Projects under Grant No. ZYYD2025ZY11 and Key Laboratory of Xinjiang Intelligent Agricultural Equipment, China for their assistance in conducting field experiments.

[References]

[1] De Oliveira Neto S S, Zeffa D M, Freiria G H, Zoz T, Da Silva C J, Zanotto M D, et al. Adaptability and Stability of Safflower Genotypes for Oil Production. Plants, 2022; 11(5): 708.

[2] Zhang Z G, Shi R M, Xing Z Y, Guo Q F, Zeng C. Improved Faster Region Based Convolutional Neural Networks (R-CNN) Model Based on Split Attention for the Detection of Safflower Filaments in Natural Environments. Agronomy, 2023; 13(10): 2596.

[3] Hu Z, Zeng H, Ge Y, Wang W, Wang J. Simulation and experiment of gas-solid flow in a safflower sorting device based on the CFD-DEM coupling method. Processes, 2021; 9(7): 1239.

[4] Guo H, Qiu Z X, Gao G M, Wu T L, Chen H Y, Wang X. Safflower picking trajectory planning strategy based on an ant colony genetic fusion algorithm. Agriculture, 2024; 14(4): 622.

[5] Zhang H, Ge Y, Sun C, Zeng H F, Liu N. Picking path planning method of dual rollers type safflower picking robot based on improved ant colony algorithm. Processes, 2022; 10(6): 1213.

[6] Ge Y, Zhang L X, Qian Y, Jiao X P, Chen Y B. Dynamic model for sucking process of pneumatic cutting-type safflower harvest device. Int J Agric & Biol Eng, 2016; 9(5): 43–50.

[7] Bac C W, Roorda T, Reshef R, Berman S, Hemming J, Van Henten E. Analysis of a motion planning problem for sweet-pepper harvesting in a dense obstacle environment. Biosystems engineering, 2016; 146: 85–97.

[8] Barth R, Hemming J, Van Henten E J. Angle estimation between plant parts for grasp optimisation in harvest robots. Biosystems Engineering, 2019; 183: 26–46.

[9] Marinoudi V, Sørensen C G, Pearson S, Bochtis D. Robotics and labour in agriculture: A context consideration. Biosystems Engineering, 2019; 184: 111–121.

[10] Tao K, Wang Z, Yuan J, Liu X. Design of a novel end-effector for robotic bud thinning of Agaricus bisporus mushrooms. Computers and Electronics in Agriculture, 2023; 210: 107880.

[11] Li M, Liu P. A bionic adaptive end-effector with rope-driven fingers for pear fruit harvesting. Computers and Electronics in Agriculture, 2023; 211: 107952.

[12] Bai Y, Zhang B, Xu N, Zhou J, Shi J Y, Diao Z H. Vision-based navigation and guidance for agricultural autonomous vehicles and robots: A review. Computers and Electronics in Agriculture, 2023; 205: 107584.

[13] Sui S S, Li M, Li Z P, Zhao Y H, Wang C Y, Du W S, et al. A comb-type end-effector for inflorescence thinning of table grapes. Computers and Electronics in Agriculture, 2024; 217: 108607.

[14] Gao J, Zhang F, Zhang J X, Yuan T, Yin J L, Guo H, et al. Development and evaluation of a pneumatic finger-like end-effector for cherry tomato harvesting robot in greenhouse. Computers and Electronics in Agriculture, 2022; 197: 106879.

[15] Gao J, Zhang F, Zhang J X, Guo H, Gao J F. Picking patterns evaluation for cherry tomato robotic harvesting end-effector design. Biosystems Engineering, 2024; 239: 1–12.

[16] Wang Y, Yang Y, Yang C H, Zhao H M, Chen G B, Zhang Z, et al. End-effector with a bite mode for harvesting citrus fruit in random stalk orientation environment. Computers and Electronics in Agriculture, 2019; 157: 454–470.
[17] Castro-Garcia S, Sola-Guirado R, Gil-Ribes J. Vibration analysis of the fruit detachment process in late-season 'Valencia' orange with canopy shaker technology. Biosystems Engineering, 2018; 170: 130–137.
[18] Van Herck L, Kurtser P, Wittemans L, Edan Y. Crop design for improved robotic harvesting: A case study of sweet pepper harvesting. Biosystems Engineering, 2020; 192: 294–308.
[19] Roshanianfard A, Noguchi N. Pumpkin harvesting robotic end-effector. Computers and Electronics in Agriculture, 2020; 174: 105503.
[20] Zhang Z, Zeng C, Xing Z, Xu P, Guo Q F, Shi R M, et al. Discrete element modeling and parameter calibration of safflower biomechanical properties. Int J Agric & Biol Eng, 2024; 17(2): 37–46.
[21] Ge Y, Zhang L X, Gu J W, Fu W, Zhu R G, Zhang H M. Parameter optimization and experiment of dual roller harvesting device for safflower. Transactions of the CSAE, 2015; 31(21): 35–42.
[22] Zhang Z G, Xing Z Y, Yang S P, Feng N, Liang R Q, Zhao M Y. Design and experiments of the circular arc progressive type harvester for the safflower filaments. Transactions of the CSAE, 2022; 38(17): 10–21.
[23] Cao W B, Yang S P, Li S F, Jiao H B, Lian G D, Niu C, et al. Parameter optimization of height limiting device for comb-type safflower harvesting machine. Transactions of the CSAE, 2019; 35(14): 48–56. DOI: 10.11975/j. issn. 1002-6819.2019. 14.006. DOI: 10.11975/j.issn.1002-6819.2019.14.006. (in Chinese)
[24] Sun C, Ge Y, Zhang H, Zeng H F, Zhang L X. Design and experiment of the vertical brush-roller picking device for dry-safflower harvesters. Transactions of the CSAE, 2023; 40(6): 203–211. (in Chinese)
[25] Xing Z Y, Zhang Z G, Shi R M, Guo Q F, Zeng C. Filament-necking localization method via combining improved PSO with rotated rectangle algorithm for safflower-picking robots. Computers and Electronics in Agriculture, 2023; 215: 108464.
[26] Huang M S, He L, Choi D, Pecchia J, Li Y M. Picking dynamic analysis for robotic harvesting of Agaricus bisporus mushrooms. Computers and Electronics in Agriculture, 2021; 185: 106145.
[27] Liu J Z, Peng Y, Faheem M. Experimental and theoretical analysis of fruit plucking patterns for robotic tomato harvesting. Computers and Electronics in Agriculture, 2020; 173: 105330.
[28] Xu X, Wang Y N, Jiang Y M. End-effectors developed for citrus and other spherical crops. Applied Sciences, 2022; 12(15): 7945.
[29] Mousaviraad M, Tekeste M. Effect of grain moisture content on physical, mechanical, and bulk dynamic behaviour of maize. Biosystems Engineering, 2020; 195: 186–197.
[30] Vu V, Ngo Q, Nguyen T, Nguyen H, Nguyen Q, Nguyen V. Multi-objective optimisation of cutting force and cutting power in chopping agricultural residues. Biosystems Engineering, 2020; 191: 107–115.
[31] Guo J, Karkee M, Yang Z, Fu H, Li J, Jiang Y L. Discrete element modeling and physical experiment research on the biomechanical properties of banana bunch stalk for postharvest machine development. Computers and Electronics in Agriculture, 2021; 188: 106308.
[32] Golzarijalal M, Ong L, Harvie D, Gras S. Experimental investigation, numerical simulation and RSM modelling of the freezing and thawing of Mozzarella cheese. Food and Bioproducts Processing, 2024; 143: 143–157.